ELSEVIER

Soil Dynamics and Earthquake Engineering 27 (2007) 586–597

SOIL DYNAMICS AND EARTHQUAKE ENGINEERING

www.elsevier.com/locate/soildyn

Shaking hazard compatible methodology for probabilistic assessment of permanent ground displacement across earthquake faults

M.I. Todorovska*, M.D. Trifunac, V.W. Lee

Department of Civil and Environmental Engineering, University of Southern California, Los Angeles, CA 90089-2531, USA

Received 9 February 2005; accepted 13 April 2006

Abstract

A methodology for probabilistic hazard assessment of permanent displacement across faults caused by earthquake rupture is presented, *compatible* with region specific models for ground shaking hazard in California, developed earlier by the authors and coworkers. Assessment of permanent dislocations across faults is important for the design and retrofit of highway bridges and tunnels crossing faults, as well as for other lifelines crossing faults, such as aqueducts, water and gas lines, etc. The methodology is illustrated for two strike-slip faults (prototypes of Class A and Class B faults in California), for 50 years exposure. The illustrations show that, for given seismic moment rate, the hazard estimates are quite sensitive to how the seismic moment is distributed over earthquake magnitudes. They also show that the hazard is small even for very small levels of displacement, in contrast to ground shaking hazard, which is due to the fact that only one fault contributes to the hazard and not every event on that fault necessarily affects the site.

Keywords: Probabilistic seismic hazard; Fault displacement hazard; Long structures; Structures crossing faults

1. Introduction

In densely populated areas near the continental margins, characterized by numerous faults with moderate to high seismic activity, situations of lifelines (highway bridges and tunnels, aqueducts, gas lines) crossing active faults are not uncommon. A well-known example is the Vincent Thomas Bridge, connecting Terminal Island and Port of Los Angeles to San Pedro and Los Angeles, which crosses the Palos Verdes Fault. Another example is the San Diego–Coronado Bay Bridge connecting San Diego and Coronado. High-resolution seismic reflection survey (conducted by California Geological Survey) has concluded that a number of strands of the Rose Canyon Fault zone could be directly beneath the main span of this bridge. There are also a number of tunnels crossing major faults in California, for example, the Bart Tunnel in Berkeley Hill, and the Clermont Water Tunnel, both crossing the Hayward Fault in northern California. Another example is the Devils Slide Tunnel on Route 1 in the San Francisco Bay area, located along the western edge of the coastal range geologic province of California, between the cities of Pacifica on the north and Monrata on the south, which is an area of high seismic activity comprising of the San Andreas Fault and San Gregorio Fault [1]. For the design and retrofit of such structures, and for the assessment of their performance during earthquakes, it is essential to have rational estimates of the permanent ground displacement caused by seismic slip.

This paper presents a model for the assessment of permanent ground displacement across a fault, due to a slip on that fault caused by an earthquake, within the framework of *probabilistic* seismic hazard analysis, hence considering the effects of all possible events on the fault, and the likelihood of their occurrence during the life (or service time) of the structure. The model predicts, for a given confidence level, the displacement across a fault (caused by an earthquake rupture) that will not be exceeded during a specified exposure period. Results are presented for the expected number and return period of exceedances, and for the probability of exceedance for a

*Corresponding author.
E-mail address: mtodorov@usc.edu (M.I. Todorovska).

0267-7261/$ - see front matter © 2006 Elsevier Ltd. All rights reserved.
doi:10.1016/j.soildyn.2006.11.002

range of values, for two hypothetical strike-slip faults, with characteristics similar to Class A and Class B faults in California, where Class A are the most active faults, with average slip rate $\dot{\bar{u}} > 5\,\mathrm{mm/year}$, and Class B are all other faults [2].

The probabilistic framework makes it possible to compare not only multiple risks to a structure caused by earthquakes, but also to compare the seismic risk with risks from other natural and man made hazards, and with other voluntary or involuntary risks to individuals and society. In comparing risks to a structure from different consequences of earthquakes, it is important that the respective methodologies for assessment of the hazards are *compatible*. The presented model is *compatible with hazard models for strong ground shaking and its consequences in California*, e.g. peak velocity, response spectrum amplitudes, peak ground strain, and soil liquefaction developed earlier by the authors of this paper [3–6].

A similar methodology for probabilistic fault displacement hazard analysis—for *normal* faulting environment (aimed at application to the potential Yucca Mountain nuclear waste repository site in Nevada)—has been presented earlier by Youngs et al. [7], who refer to it as an "earthquake approach," and also present the "displacement approach," in which a rate of occurrence of displacement events is defined explicitly, without the involvement of earthquake magnitude. Our methodology is conceptually the same as the "earthquake approach" of Youngs et al. [7], but differs in the scaling law used to estimate the conditional probability of exceedance of levels of displacement given an earthquake has occurred. In our case, this scaling law is specific for faults in California, which is in a shallow seismogenic zone with predominantly *strike-slip* mechanism of faulting. Another important difference is that our model is *compatible* with scaling laws for prediction of ground shaking hazard (peak amplitudes, spectra, peak ground strain, and occurrence of soil liquefaction). Earlier, Stepp et al. [8] presented results for fault displacement hazard at the Yucca Mountain site in Nevada, without a detailed description of the methodology.

2. Methodology

The methodology is a special case of probabilistic seismic hazard assessment of some adverse consequence of earthquakes, such as a characteristic of ground shaking exceeding some level, or occurrence of liquefaction, and is based on specification of a probabilistic model for earthquake occurrence, and conditional probability that the adverse event will occur, given that an earthquake has occurred. The assessment of hazard for permanent displacement across a fault is simpler in that it involves only one earthquake source zone, while ground shaking hazard involves many such zones. Another simplification is that not every earthquake occurring in the source zone would affect the site, while every earthquake would cause some level of shaking, depending on the distance. Hence, the assessment of fault displacement hazard requires specification of an additional conditional probability—that the event that has occurred affects the site—but the estimation of the effect is simpler in that it does not depend on the distance to the source (which is zero), although in reality it does depend on the location of the site along the rupture. For example, the displacement is nonuniform along the rupture length, and may be discontinuous. The static displacement field decreases with distance from the fault. However, typical bridge span is small, of the order of 100 m, and this "attenuation" effect is small compared to the overall uncertainty of the estimation. Hence, we estimate the displacement immediately across the fault.

Part (a) of Fig. 1 shows a fault with length L and width W, dipping at angle δ, and extending from the ground surface to depth $H = W \sin\delta$. Part (b) shows the fault surface, the site (at distance x from the center of the fault), and three possible ruptures, one of which affects the site, another one that occurs at depth and does not break the ground surface, and a third one that breaks the ground surface but does not extend horizontally to the site. The possible ruptures have lengths $L_R(M)$ and widths $W_R(M)$, which both depend on magnitude.

Let D be a random variable representing, for an earthquake that has ruptured the ground surface, the absolute value of the displacement across the rupture at the ground surface, and D_{site} be the same type of displacement *at the site*, which may or may not have been affected by the

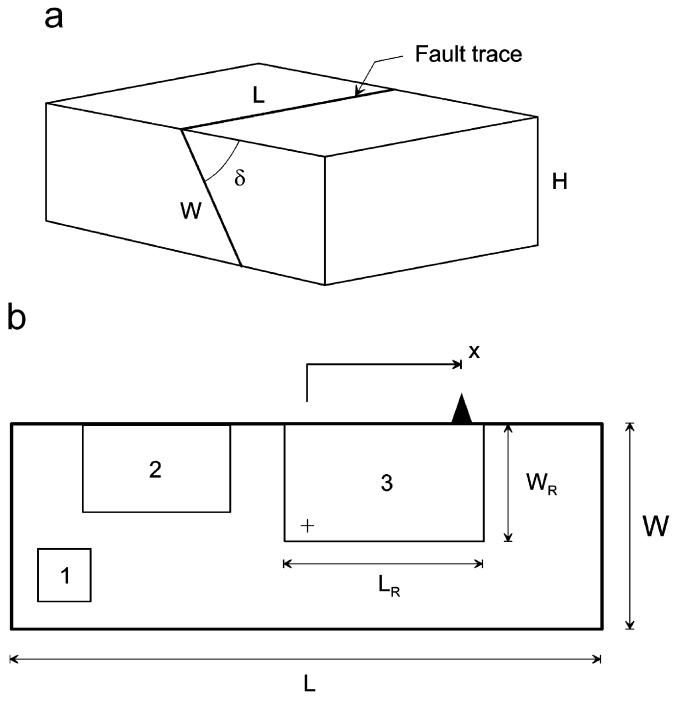

Fig. 1. (a) Model geometry; (b) the fault surface and three possible ruptures, only one of which (no. 3) affects the site (no. 1 does not break the surface and does not extend horizontally to the site; no. 2 breaks the surface but does not extend to the site).

earthquake, and let $p(d,t)$ be the probability that D_{site} exceeds level d during exposure period t

$$p(d,t) = P\{D_{\text{site}} > d|t\}. \tag{1}$$

Being a direct consequence of an earthquake occurrence, the probabilistic model for this event is determined by the probabilistic model of earthquake occurrence. The following two sections derive the model, respectively, for Poissonian earthquakes and for earthquakes occurring at a time dependent rate.

3. Hazard model for Poissonian earthquakes

Assuming that the earthquakes on the fault occur independently of one another, their number during specified exposure is Poissonian and their return period is an exponential random variable. For practical purposes, let us discretize the magnitudes of possible earthquakes, and let $M_i,\ i = 1,\ldots,N_i$ be the possible magnitudes, and $n_i(t)$ be the corresponding expected number of earthquakes during exposure t. Then, the event $\{D_{\text{site}} > d \mid t\}$ is a selective Poissonian process with rate that is a prorated value of the earthquake occurrence rate (for the fact that not every rupture will break the surface and extend to the site, and even if it does, the displacement may not exceed level d). Due to the statistical independence, the exceedance rate is a sum of the exceedance rates for the individual magnitude levels, and can be written as

$$m(d,t) = \sum_{i=1}^{L} q_i(d) n_i(t), \tag{2}$$

where $m(d,t)$ is the expected number of exceedances during exposure period t from all such events. The magnitude dependent prorating factor $q_i(d)$ is the conditional probability that the displacement (across the fault) *at the site* will exceed level d given that an earthquake of magnitude M_i has occurred on the fault, which can be estimated as follows:

$$\begin{aligned} q_i(d) &= P\{D_{\text{site}} > d|\ \text{event } M = M_i \text{ occurred}\} \\ &= P\{D > d \mid \text{ event } M = M_i \text{ occurred}\} \\ &\quad \times P\left\{\begin{array}{l}\text{rupture breaks}\\ \text{ground surface}\end{array}\right\} \\ &\quad \times P\left\{\begin{array}{l}\text{rupture extends}\\ \text{horizontally to the site}\end{array}\right\}. \end{aligned} \tag{3}$$

Then the return period of exceedance of level d during exposure t during these events is exponentially distributed, with average value $t/m(d,t)$, and the probability of this event is

$$\begin{aligned} p(d,t) &= P\{D_{\text{site}} > d \mid t\} \\ &= 1 - \mathrm{e}^{-m(d,t)}. \end{aligned} \tag{4}$$

The remaining part of this section examines the earthquake rates specification and the conditional probability $q_i(d)$.

The rates for the Poissonian earthquakes in a source zone usually are specified to follow a truncated liner Gutenberg–Richter law

$$\log N(M) = a - bM, \quad M \leqslant M_{\max}, \tag{5}$$

where $\int_{M-\Delta M/2}^{M+\Delta M/2} N(m)\,\mathrm{d}m$ is the average number of earthquakes per year of magnitude within the interval $(M - \Delta M/2, M - \Delta M/2)$, $M_{\max}$ is the maximum magnitude for the fault, and a and b are constants. Other shapes of Gutenberg–Richter law that deviate from the linear law can also be specified. Then

$$n_i(t) = t \int_{M_i-\Delta M/2}^{M_i+\Delta M/2} N(m)\,\mathrm{d}m, \tag{6}$$

where ΔM is the discretization interval. The Poissonian process is memoryless, and is completely defined by the average rate.

4. Hazard model for earthquakes with time dependent hazard rate

It has been observed that some faults, tend to produce large earthquakes more frequently than predicted by a truncated linear Gutenberg–Richter fit to observed seismicity data. Also, consistent with the elastic rebound theory of earthquakes, the chance of a large earthquake on a fault depends on the time elapsed since the previous one, as it takes time to replenish the strain energy to generate another large earthquake. This has been the basis for the characteristic earthquake model [9], where the characteristic earthquake for a fault is the one that ruptures the entire fault, and the likelihood of the next event depends on the time elapsed since the previous such event. Such processes can be modeled as a one step memory renewal process, e.g. with lognormally distributed return period [10], and require an additional input parameter—the time elapsed since the previous such event, t_0. Due to lack of data and lack of regularity in the occurrence of large earthquakes (either the segment or the magnitude is not repeated), uncertainty in the segmentation, and the interaction between neighboring segments and possibility of a joint rupture in a large earthquake, this time dependent model has been applied to a small number of faults, mostly along the plate boundaries, and the time until the next characteristic event is often modeled as an exponential random variable.

The following reviews briefly a time dependent characteristic earthquake model, described as a *generalized Poissonian* process [11]. This model assumes, like in the Poissonian process, that the earthquake occurrence in time is *orderly*, i.e. the probability of more than one event in a short time interval is negligible. Let $\lambda(t,t_0)$ be a time dependent occurrence rate for the characteristic earthquake. Then the expected number of events in time interval

t (set to zero at the time of the previous such event) is

$$n(t \mid t_0) = \int_0^t \lambda(\tau, t_0)\,\mathrm{d}\tau \tag{7}$$

the average number of exceedances of level d from such earthquakes is

$$m(d, t \mid t_0) = q_i(d) n(t \mid t_0) \tag{8}$$

the corresponding probability of exceedance is

$$p(d, t \mid t_0) = 1 - \mathrm{e}^{-m(d, t \mid t_0)} \tag{9}$$

and the number of exceedances during exposure t is again Poissonian.

5. Combined effect of all earthquakes

Assuming that the occurrence of smaller magnitude earthquakes is Poissonian, and is statistically independent of the characteristic earthquakes, which occur as a generalized Poissonian process, the number of exceedances of level d is also generalized Poissonian, with the expected number of exceedances, $m_{\mathrm{tot}}(t \mid t_0)$, equal to the sum of the expected number of exceedances from Poissonian, $m_{\mathrm{Pois}}(t)$, and characteristic earthquakes, $m_{\mathrm{ch}}(d, t \mid t_0)$,

$$m_{\mathrm{tot}}(t \mid t_0) = m_{\mathrm{Pois}}(t) + m_{\mathrm{ch}}(d, t \mid t_0) \tag{10}$$

and the corresponding probability of exceedance is

$$p(d \mid t_0) = 1 - \mathrm{e}^{-m_{\mathrm{tot}}(d, t \mid t_0)}. \tag{11}$$

A more general relation to compute the probability of exceedance from any event, including a prediction based on expert judgment is

$$p(d, t) = 1 - \prod_j [1 - p_j(d, t)], \tag{12}$$

where $p_j(d, t)$ are the probabilities of exceedance from the individual events or populations of events described by same type of probabilistic model.

6. Probability that the rupture breaks the ground surface and extends to the site

The likelihood that a rupture will break the ground surface can be estimated specifically for a fault based on: direct observations during prior earthquakes, the hypocentral depth distribution during past earthquakes, relations for rupture width versus earthquake magnitude, etc. For the purpose of demonstrating the methodology, in this paper we assume that the likelihood that a rupture will extend to the ground surface is larger for larger magnitude earthquakes, which have larger rupture width, $W_{\mathrm{R}}(M)$, compared to the width of the fault, W, and we adopt

$$P\left\{\begin{array}{l}\text{rupture breaks}\\ \text{ground surface}\end{array}\right\} = \min\left(1, \frac{W_{\mathrm{R}}(M)}{W}\right) \equiv r_W(W, W_{\mathrm{R}}). \tag{13}$$

Similarly, we assume that the likelihood that the ruptured segment of the fault, $L_{\mathrm{R}}(M)$, would extend to the site would be larger for larger magnitude earthquakes, which have longer rupture length, but would also depend on where the site is located relative to the edges of the fault (due to the constraint that the rupture has to fit along the fault length, L). Let us assume equal likelihood that a rupture will occur anywhere along the length of the fault, as long as it fits within the fault length. Then

$$P\left\{\begin{array}{l}\text{rupture extends}\\ \text{horizontally to the site}\end{array}\right\} = \begin{cases} 1, & L_{\mathrm{R}}(M) \geqslant L \\ \min\left(1, \dfrac{L_{\mathrm{R}}(M)}{L - L_{\mathrm{R}}(M)}\right), & L_{\mathrm{R}}(M) < L, \\ & |x| \leqslant \dfrac{L}{2} - L_{\mathrm{R}}(M) \\ \min\left(1, \dfrac{\frac{L}{2} - |x|}{L - L_{\mathrm{R}}(M)}\right), & L_{\mathrm{R}}(M) < L, \\ & |x| > \dfrac{L}{2} - L_{\mathrm{R}}(M) \end{cases} \equiv r_L(L, L_{\mathrm{R}}, x), \tag{14}$$

where $|x|$ is the distance of the site from the center of the fault (see Fig. 1). In Eq. (14), $|x| \leqslant (L/2) - L_{\mathrm{R}}(M)$ corresponds to a site close to the center of the fault, while $|x| > (L/2) - L_{\mathrm{R}}(M)$ corresponds to a site close to one end, and the classification of the site in these two categories depends on the rupture length, which in turn depends on the earthquake magnitude.

7. Regression models for rupture length and width

The rupture size grows exponentially with earthquake magnitude, but the rate of growth along the fault length and width depends on the type of seismogenic zone. For example, in the shallow seismogenic zone of California, the rupture length and width, L_{R} and W_{R}, grow proportionally for small magnitudes. For larger magnitudes, the rupture width is limited by the width of the seismogenic zone (~18 km), while the rupture length can grow further. For the purpose of estimating probabilities r_W and r_L, as given in Eqs. (13) and (14), we initially considered using the published relations for L_{R} and W_{R} of Trifunac [12,13], and of Wells and Coppersmith [14], but opted for our own relations

$$\log_{10} L_{\mathrm{R}}(M) = 0.5113M - 1.9341 \tag{15}$$

and

$$\log_{10} W_{\mathrm{R}}(M) = 0.2292M - 0.5128 \tag{16}$$

which we derived by least squares fit through a subset of the data gathered by Wells and Coppersmith [14] that corresponds to California earthquakes. Fig. 2 shows L_{R} and W_{R} versus magnitude for model 3 of Trifunac [12,13]

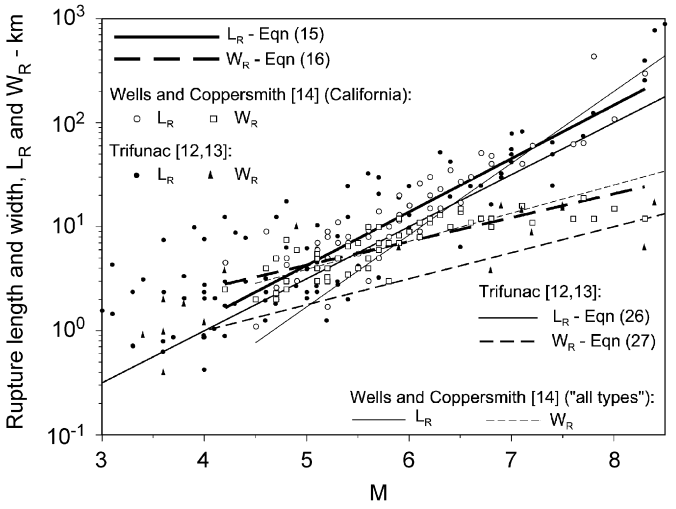

Fig. 2. Data and empirical scaling laws for rupture length and width, L_R and W_R versus earthquake magnitude. The heaviest lines correspond to Eqs. (15) and (16) that were used to estimate probabilities r_L and r_W that the rupture will extend horizontally to the site and will break the ground surface. The medium heavy lines correspond to L_R and W_R proposed by Trifunac [12,13], which are consistent with the model for prediction of the permanent displacement across the fault, and the weak line correspond to L_R and W_R proposed by Wells and Coppersmith [14] for all types of faulting.

(the medium thick lines), consistent with *seismological* estimates of rupture length and width, with theoretical earthquake source models, and with empirical scaling models of peaks and spectra of strong ground motion [12,15]. For this model, L_R and W_R grow proportionally with magnitude up to $M = 4$, after which W_R grows at a smaller rate. Fig. 2 also shows empirical relations for L_R and W_R of Wells and Coppersmith [14] (the thin lines) for "all" types of faulting, derived from worldwide data, and valid for $4.8 \leqslant M \leqslant 7.9$. The open circles and rectangles show a subset of the data for L_R and W_R gathered by Wells and Coppersmith [14] for earthquakes in California. The corresponding full symbols show data gathered by Trifunac [12,13] from various published seismological estimates. The thick lines represent L_R and W_R as defined in Eqs. (15) and (16), which will be used to estimate probabilities r_L and r_W. It can be seen that these models have slopes similar to the slopes of the models of Trifunac [12,13] models, and are in general agreement with the data gathered by Trifunac [12,13].

The uncertainty in the estimates of $L_R(M)$ and $W_R(M)$ can be incorporated as follows:

$$P\left\{\begin{array}{l}\text{rupture breaks}\\ \text{ground surface}\end{array}\right\} = \int_0^\infty r_W(W,y) f_{W_R}(y)\,\mathrm{d}y, \tag{17}$$

$$P\left\{\begin{array}{l}\text{rupture extends}\\ \text{horizontally to the site}\end{array}\right\} = \int_0^\infty r_L(W,y) f_{L_R}(y)\,\mathrm{d}y, \tag{18}$$

where $f_{L_R}(y)$ and $f_{W_R}(y)$ are, respectively, the probability density functions of $L_R(M)$ and $W_R(M)$.

8. Regression model for seismic displacement across the fault

The most delicate part of the hazard model is the choice of scaling law for the permanent displacement across the fault. We considered adopting one of the published models, in particular, those of Wells and Coppersmith [14], and the models for $d_{\max}$ of Lee et al. [15], or developing a new model.

Wells and Coppersmith [14] present models that are linear, fits through worldwide data for the logarithm of surface displacement versus earthquake magnitude, separately for different types of faulting, and also for all types of faulting, valid within the range of the data. For example, for the case of "all" types of faulting (for which the regression is most stable due to the largest number of data points) they use data from 148 events, and their model is valid for magnitudes between 5.6 and 8.1. The standard deviation of the logarithm of the displacement for this regression is 0.36, or a factor of 2.3, which is comparable to the scatter of the scaling laws for prediction of amplitudes of ground shaking.

The models for $d_{\max}$ of Lee et al. [15] predict peak ground displacement as a function of earthquake magnitude, distance from the source, propagation type characteristics, and various combinations of geologic site and local soil conditions. Their models were derived by multistep regression of strong motion data of peak ground displacement (computed from recorded accelerograms, after correction for the reduction due to baseline correction and high-pass filtering). They used about 2000 three-component accelerograms recorded in the Western US, and imposed a constraint such that *on the fault* (at zero epicentral distance) the predicted displacements are consistent with fault dislocation data. Based on extrapolations using physical source models, their models are valid for all magnitudes, and predict decay with distance near the source consistent with a theoretical model of radiation from a dislocation. Further, these models are also consistent with the long period asymptote of the frequency dependent attenuation models of Lee and Trifunac [16,17] of ground motion in the near field. The scatter of their model is such that the standard deviation of $\log_{10} d_{\max}$ is 0.38, or a factor of 2.4.

We opted for adopting one of the models of Lee et al. [15] because of their consistency with the models for prediction of ground shaking hazard. This consistency is important for structures that are sensitive both to ground shaking and to static displacements. As the uncertainty in the prediction of ground motion amplitudes and permanent displacement remains relatively large (greater than a factor of two), for meaningful comparison and weighting of different hazards and their consequences upon the structure, it is essential that the scaling laws are compatible.

The following describes in detail the *Mag + site + soil + %rock path* model of Lee et al. [15], that was adopted for

the hazard model presented in this paper. Their other models differ by the particular combination of site (and path) parameters used in the regression. We assume symmetric rupture, so that the relative displacement of two points (at the ground surface) on the opposite sides of the fault, D, is twice the absolute displacement on either side of the fault

$$D = 2d_{\max}. \tag{19}$$

While D varies along the length of the rupture, and may be discontinuous, we assume in the model that it represents the *average* over the length of the rupture. For epicentral distances $R<140$ km, Lee et al. [15] give $d_{\max}$ in cm as

$$\begin{aligned}\log_{10} d_{\max} &= M - 2.2470\log_{10}(\Delta/L_R) + 0.6489M + 0.0518s \\ &\quad - 0.3407v - 2.9850 \\ &\quad - 0.1369M^2 + (-0.0306S_L^1 + 0.2302S_L^2 + 0.5792S_L^3) \\ &\quad + [-0.3898r - 0.2749(1-r)]R/100,\end{aligned} \tag{20}$$

where M is the earthquake magnitude, R is epicentral distance (in km), Δ is "representative" source to station distance (defined in the next paragraph), L_R is rupture length, v is direction of motion indicator ($v=0$ for horizontal motion, and $v=1$ for vertical motion), r is ratio of horizontal wave path traveled through rock, s is geologic site condition indicator ($s=0$ for sediments, $s=2$ for geologic rock and $s=1$ for sites that cannot be clearly classified in the first two groups), and S_L^1, S_L^2 and S_L^3 is local soil condition indicators, related to the soil site parameter s_L ($S_L^1=1$ if "rock" soil or "stiff" soil condition, and zero otherwise; $S_L^2=1$ if "deep" soil condition and zero otherwise; $S_L^3=1$ if "deep cohesionless soil" condition and zero otherwise).

The "representative" source to station distance, first proposed as a concept by Gusev [18], depends both on physical distance and on the size of the rupture, and is defined as

$$\Delta = S\left(\ln\frac{R^2+H_R^2+S^2}{R^2+H_R^2+S_0^2}\right)^{-1/2}, \tag{21}$$

where H_R is the focal depth, S is source dimension, and S_0 is source coherence radius. For small epicentral distances ($R<5$ km), the source dimension, S, is given by

$$S = \begin{cases} 0.0729(5.5-M)10^{0.5M}, & M<4.5, \\ -25.34+8.51M, & 4.5\leqslant M\leqslant 7.25. \end{cases} \tag{22}$$

The source coherence radius, S_0, as seen at the site, depends on the frequency of the radiated energy and on the distance from the source. Gusev [18] and Lee et al. [15] approximate S_0 by

$$S_0 \sim \beta T/2, \tag{23}$$

where β is the velocity of shear waves in the source region, and T is period of "predominant" wave motion, i.e. the period of the largest amplitudes of the Fourier spectrum of displacement. The shape of this spectrum depends on the distance from the source, and on the corner frequencies f_1 and f_2, which are related to rupture length L_R and width W_R [12,13]. As per statistical studies of strong ground motion [19], for unilateral faulting, f_1 is related to the total duration of faulting, τ_1, and f_2 is related to the time of spreading of the dislocation over the entire rupture width, τ_2, as

$$\tau_1 \sim 1/f_1 = L_R/2.2 + W_R/6, \tag{24}$$

$$\tau_2 \sim 1/f_2 = W_R/6. \tag{25}$$

The rupture length and width used in Eqs. (24) and (25) are those of Trifunac [12,13]

$$\log_{10} L_R(M) = 0.5M - 2 \tag{26}$$

and

$$\log_{10} W_R(M) = \begin{cases} L_R, & M\leqslant 4.25, \\ 0.25M-1, & M>4.25 \end{cases} \tag{27}$$

which are consistent with data from *seismological* estimates of rupture dimensions, and with strong motion estimates of ground motion (see Fig. 2 and Ref. [12]).

For scaling of peak displacement, Lee et al. [15] assume "predominant" period for the estimation of source coherence radius $T\approx\tau_1/2$ to $\tau_1/3$. Then, for $\beta\sim 3$ km/s

$$S_0 = \tfrac{1}{2}\min(S_f, S), \tag{28}$$

where S is the source dimension, given by Eq. (22), and S_f is

$$S_f = \begin{cases} L_R(M), & M<3.5, \\ L_R(M)/2.2 + W_R(M)/6, & 3.5<M\leqslant 7, \\ L_R(M_{\max})/2.2 + W_R(M_{\max})/6, & M>M_{\max}=7 \end{cases} \tag{29}$$

with $L_R(M)$ and $W_R(M)$ as defined in Eqs. (15) and (16).

For estimation of permanent displacement, we evaluate $d_{\max}$ at epicentral distance $R=0$, hypocentral depth $H_R = 0.5W_R\sin\delta$ (see Fig. 1), and for the following path and site conditions: $r=1$ (entire travel path through rock), $s=2$ ("rock" geologic site condition) and $s_L=0$ ("rock" local soil condition). Lee et al. [15] also analyzed the distribution of the residuals of $\log_{10} d_{\max}$, and showed that a normal distribution with mean -0.0090 and the standard deviation 0.3975 is reasonably close to the actual distribution. Hence, $D=2d_{\max}$ is modeled as a lognormal random variable, such that $\log_{10} D$ has mean μ and standard deviation σ

$$\begin{aligned}\mu &= M - 2.2470\log_{10} \\ &\quad \times[\Delta(M, R=0, H_R=0.5W_R\sin\delta, S, S_0)/L_R] + 0.6489M \\ &\quad + 0.0518^*2 - 0.3407v - 2.9850 - 0.1369M^2 - 0.0306 \\ &\quad + \log_{10} 2 - 0.0090,\end{aligned} \tag{30}$$

$$\sigma = 0.3975, \tag{31}$$

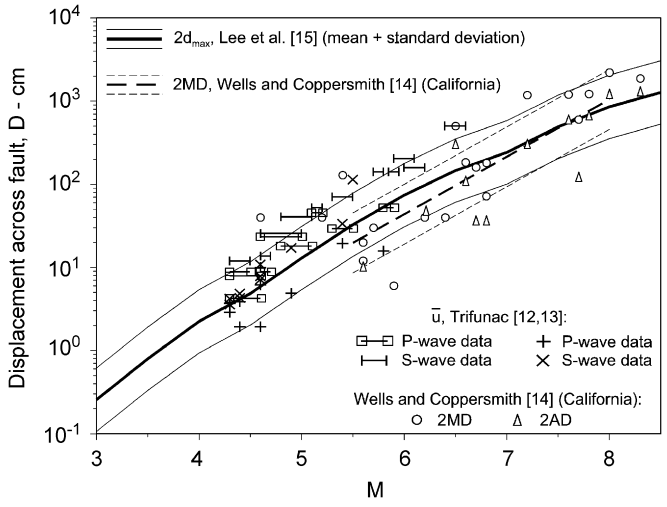

Fig. 3. Data on fault dislocation for earthquakes in California, and scaling laws for prediction of displacement at the ground surface across the fault, D, versus earthquake magnitude. The solid heavy line corresponds to the model used in this study, which is one of the models of Lee et al. [15] evaluated at zero epicentral distance. The thinner dashed line corresponds to the law for maximum displacement (MD) for all types of faulting derived by Wells and Coppersmith [14].

where L_R, W_R, S, and S_0 are all functions of magnitude, and the conditional probability of exceedance is

$$P\left\{ D>d \,\middle|\, \begin{array}{l}\text{event } M=M_l \text{ occurred}\\ \text{and ruptured the surface}\end{array}\right\} = \frac{1}{\sqrt{2\pi}\sigma}\int_{-\infty}^{\log d} \mathrm{e}^{-1/2((\log x-\mu)/\sigma)^2}\,\mathrm{d}x. \quad (32)$$

Fig. 3 shows $D=2d_{\max}$ versus magnitude, as predicted by the model (the thick lines), against the data for average dislocation, $\bar{u}$, gathered by Trifunac [12,13], and the data for average (AD) and maximum (MD) displacement gathered by Wells and Coppersmith [14] for California earthquakes. It can be seen that the model is in good agreement with the data. This figure also shows the regression model of Wells and Coppersmith [14] (the weaker lines) for AD for "all" types of faulting.

9. Results and analyses

The model is illustrated by results for two hypothetical vertical strike-slip faults, I and II, which have same length, $L=100$ km, but differ by their activity (fault II is more active) and by the manner in which the seismic moment rate is distributed over magnitudes. Fault I represents a Class B, and fault II—a Class A fault in California, where Class A are those faults with average slip rate $\dot{\bar{u}}>5$ mm/year, and Class B are all other faults [2]. In the 2002 revision of the national seismic hazard maps [2,20], for the Class A faults, 100% of the seismic moment is assigned to characteristic events, while for Class B faults, $\frac{2}{3}$ of the moment is assigned to characteristic events and $\frac{1}{3}$—to Gutenberg–Richter events, with $b=0.8$. The seismic moment rate is defined as

$$\dot{M}_0=\mu A\dot{\bar{u}}, \quad (33)$$

where A is the area of the fault and $\mu\sim 3\times10^{11}$ dyne/cm^2 is the shear modulus for the region [21]. For our hypothetical Class B fault, we follow the $\frac{2}{3}$ and $\frac{1}{3}$ partitioning of seismic moment between characteristic and Gutenberg–Richter events, while, for the hypothetical Class A fault, we consider three variants of distribution of seismic moment—one of which is partitioning as for Class B faults, and the other two are 100% assignment to characteristic events—and examine their effect on the final result. For both faults, the magnitude of the characteristic events is distributed near the maximum magnitude for the fault, with average occurrence rates over this range decreasing with magnitude according to a Gutenberg–Richter law with $b=0.5$. The return period of the characteristic events is assumed to be an exponential random variable, as time dependent hazard is out of the scope of this study.

The properties of the hypothetical faults I and II are summarized in Tables 1 and 2. It can be seen that both faults are vertical and shallow, and are 100 km long. For fault II, three variants of the distribution of seismic moment assigned to the fault are specified, IIa–IIc. In the results that follow, for hypothetical fault I, we compare the contributions to the hazard from the two earthquake populations at a site at the center of the fault, and we compare the hazard at sites that are at different locations along the fault. Similarly, for fault II, we compare the hazard for the three variants of distribution of seismic moment. Results are shown for: (a) the expected number of exceedances in 50 years; (b) the return periods of exceedances, and (c) the probability of exceedance, all versus different levels of displacement across the fault, d. The range of d is from as small as 1 mm to as large as 100 m, to examine the asymptotic trends.

Fig. 4 shows, for hypothetical fault I: (a) the distribution over magnitudes of the expected number of earthquakes in 50 years exposure, for discretization interval $\Delta M=0.5$, and (b) probabilities r_W and r_L that the rupture will break the surface and will extend horizontally to the site (see Eqs. (13) and (14)) for $x=0,10,25,40$ and 49 km. The trend seen from part (b) is that, in general, the probability of being affected by a rupture grows with magnitude, and is larger for sites closer to the center of the fault ($x=0$). However, for sufficiently small magnitudes (how small it depends on x), this probability does not depend on the

Table 1
Parameters for hypothetical fault I (Class B)

$L=100$ km, $H=13$ km, $\delta=90^\circ$	
G–R	Characteristic
$\dot{M}_0=38\times10^{22}$ dyn × cm/yr $b=0.8$, $M_{\max}=7.5$	$\dot{M}_0=75\times10^{22}$ dyn × cm/yr $b=0.5$, $6.5<M<7.5$

Table 2
Parameters for hypothetical fault II (Class A)

$L = 100\,\text{km}, H = 18\,\text{km}, \delta = 90^\circ$		
	G–R	Characteristic
IIa	$\dot{M}_0 = 4.45 \times 10^{24}$ dyn × cm/yr $b = 0.8, M_{\max} = 7.5$	$\dot{M}_0 = 8.9 \times 10^{24}$ dyn × cm/yr $b = 0.5, 6.75 < M < 7.75$
IIb		$\dot{M}_0 = 13.35 \times 10^{24}$ dyn × cm/yr $b = 0.5, 6.75 < M < 7.75$
IIc		$\dot{M}_0 = 13.35 \times 10^{24}$ dyn × cm/yr $b = 0.5, 7.25 < M < 7.75$

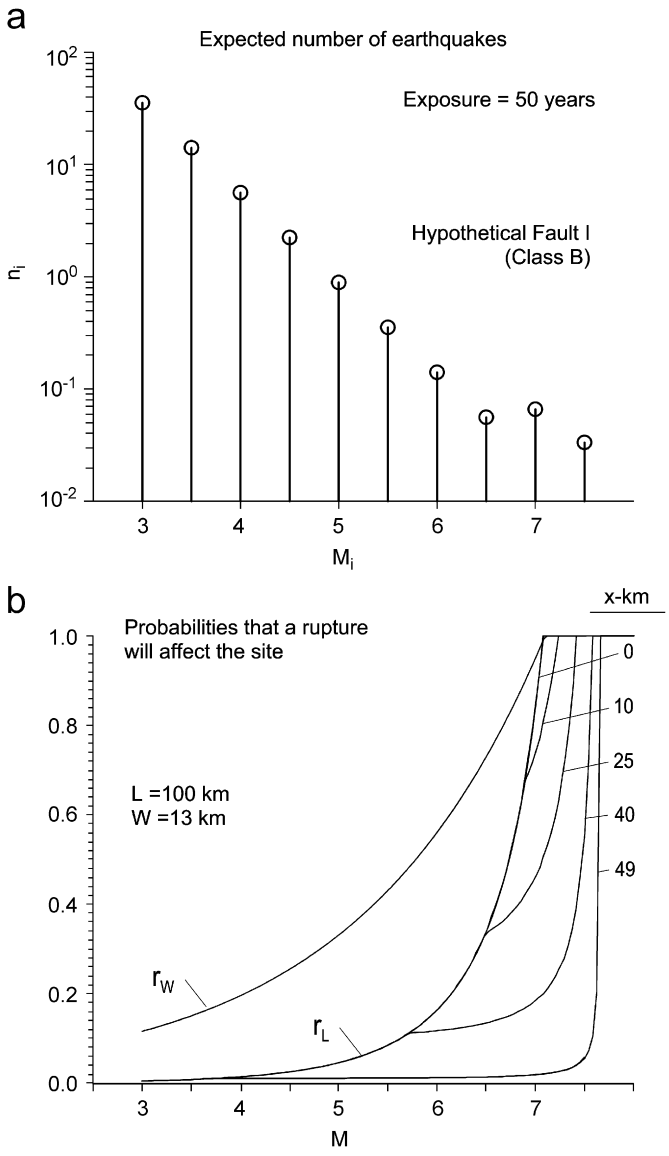

Fig. 4. Hypothetical fault I (Class B): (a) expected number of earthquakes versus magnitude for 50 years exposure (see Table 1), and (b) probabilities that a rupture will affect the site.

location of the site, as only a fraction of such earthquakes could affect any site on the fault. For larger magnitudes, this probability becomes larger for a site at the center. For very large magnitudes, as $L_R(M) \to L$, the trend is that all sites on the fault would be affected, i.e. $r_L(M) \to 1$ for all x. However, as a result of discretization of the magnitude, the largest discrete magnitude is smaller than $M_{\max}$, which results in $r_L(M) < 1$ for sites sufficiently far from the center. Results for the hazard on this fault are shown in Figs. 5 and 6.

Fig. 5 compares the contributions to the hazard from all events with that only from the Gutenberg–Richter and only from the characteristic events, for a site at the center of the fault ($x = 0$). As it can be expected, the hazard is smaller for larger levels of d, and it rapidly decreases with d for values greater than several meters. It can be seen that, for significant level of d (larger than several cm), the contribution to the hazard from the characteristic events population (i.e. larger magnitude events) is larger than the one from the Gutenberg–Richter events population. As a result of the small seismicity and the fact that not every earthquake affects the site, the hazard is generally small. For example, for $d = 50\,\text{cm}$, the probability of exceedance $p \approx 0.1$, and the return period is about 500 years.

Fig. 6 compares the hazard for sites at different distances from the center of the fault, at $x = 0, 25$ and 40 km. It can be seen that the hazard is the largest for the site at the center, and is slightly smaller for the site at $\frac{1}{4}$ fault length distance from the edge ($x = 25\,\text{km}$). The difference between the hazard at these three sites decreases with increasing level of d for which the hazard is very small everywhere along the fault. For $d = 50\,\text{cm}$, the probability of exceedance drops from $p = 0.1$ at $x = 0$ to less than half of that value at $x = 40\,\text{km}$.

Fig. 7 shows, for hypothetical fault II (a) the distribution over magnitudes of the expected number of earthquakes in 50 years exposure for the three variants of distribution of seismic moment, IIa–IIc (see Table 2), and (b) probabilities r_W and r_L, and their product, for a site at the center of the fault ($x = 0$). We recall that for models IIb and IIc, all earthquakes are characteristic. It can be seen from part (a) that, due to the specific discretization scheme adopted, the characteristic earthquakes for variants IIa and IIb have magnitude $M = 7$ and 7.5, while for variant IIc, they have only magnitude $M = 7.5$, and their number is small, despite the fact that all of the seismic moment is assigned to characteristic events, because of the very large moment release for large magnitudes, which grows exponentially with magnitude. In part (b), the probability r_L is same as for fault I, as both faults have same length, while probability r_W is smaller for this fault because of the larger width of this fault. Because of this fact, even for magnitude $M = 7.5$, according to the model adopted for this illustrations, though large, the probability that the rupture will break the surface is less than 1.

Fig. 8 shows results for the hazard for the three variants of distribution of seismicity, all corresponding to same

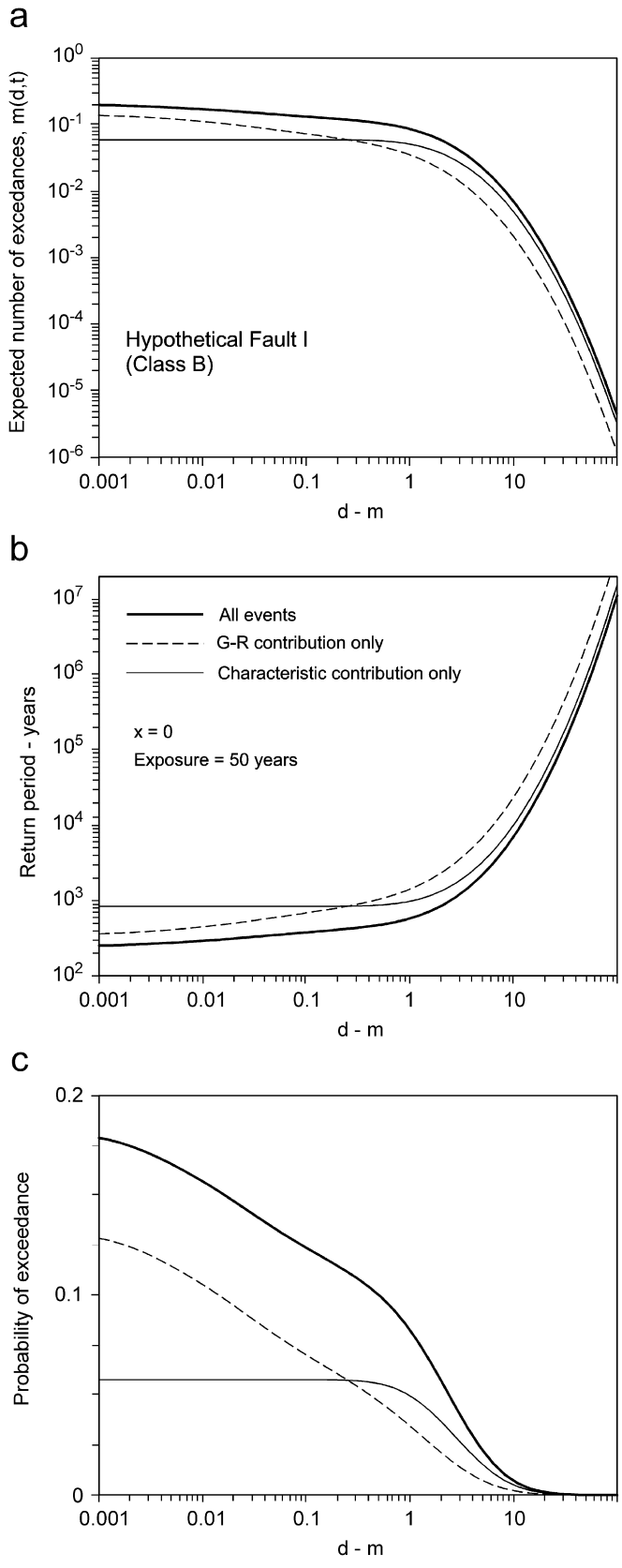

Fig. 5. Results at a site at the center of the fault for hypothetical fault I (Class B): (a) expected number of exceedances of level d during 50 years exposure; (b) return period of exceedance of level d, and (c) probability of exceedance in 50 years. The different lines correspond to estimates when all events contribute to the hazard, and when only the Gutenberg–Richter events or the characteristic events contribute to the hazard.

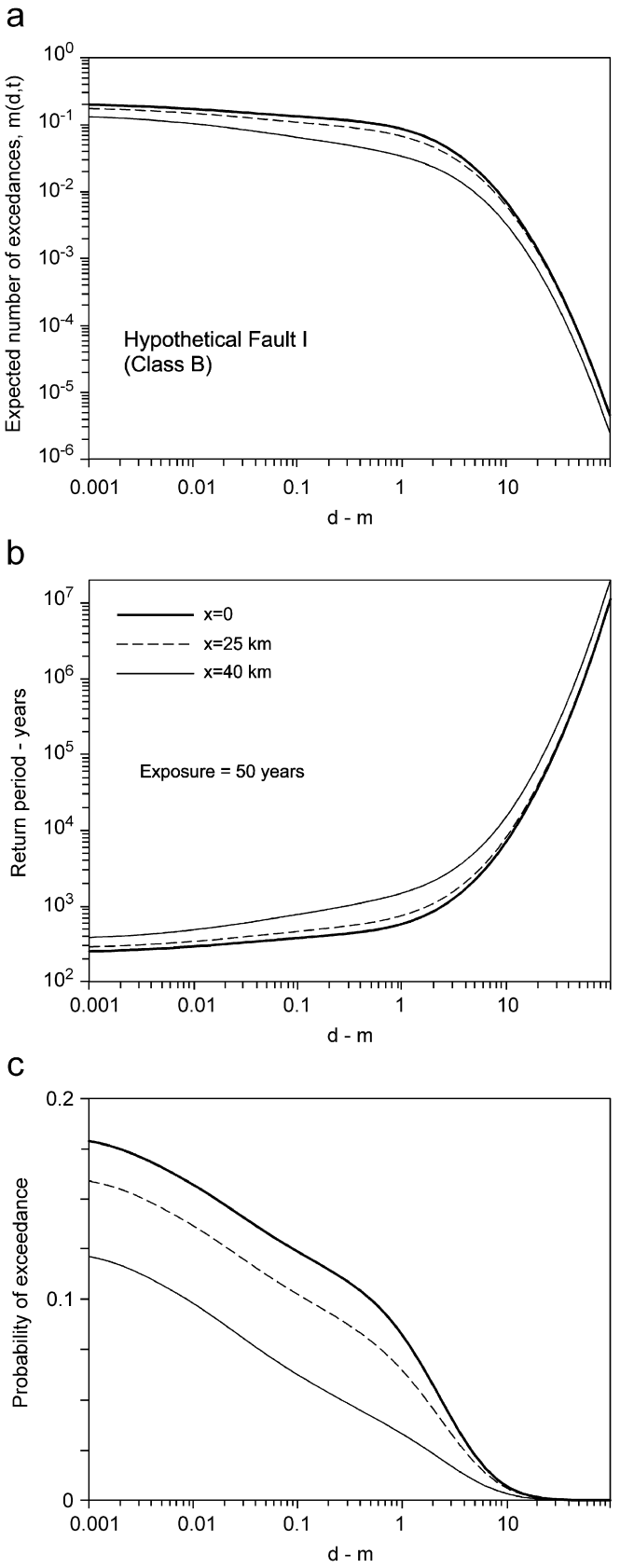

Fig. 6. Results for hypothetical fault I (Class B): (a) expected number of exceedances of level d during 50 years exposure; (b) return period of exceedance of level d, and (c) probability of exceedance in 50 years. The different lines correspond to sites at different distances, x, from the center of the fault.

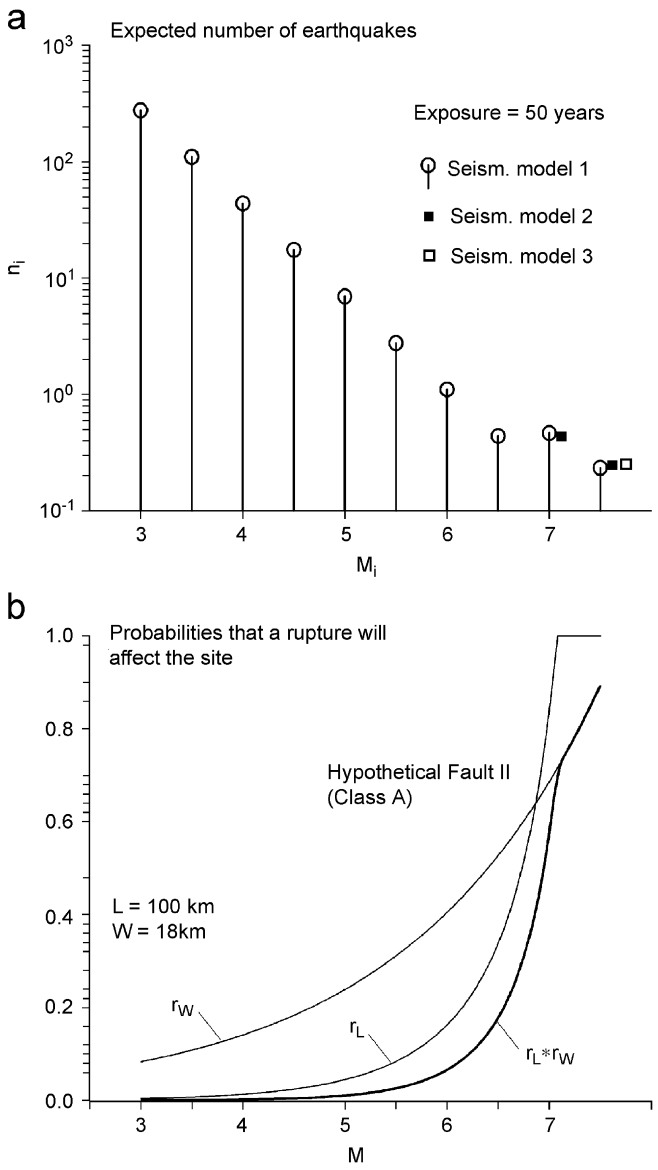

Fig. 7. Hypothetical fault II (Class A): (a) expected number of earthquakes versus magnitude for 50 years exposure (see Table 2), and (b) probabilities that a rupture will affect the site.

overall expected seismic energy release during the exposure period, and maximum magnitude. It can be seen that the hazard is the largest for variant IIa, for which $\frac{1}{3}$ of the seismic moment is assigned to Gutenberg–Richter events, and is the smallest for variant IIc, for which the characteristic events, to which all the moment is assigned to, are distributed over a shorter magnitude interval near the maximum magnitude (Table 2). This can be explained by the significantly smaller expected number of events, which is not compensated for sufficiently by their bigger effects, except for the very high levels of displacement, for which the results of all three models become the same. It can also be seen that the results for d less than several tens of centimeters, the hazard for variants IIb and IIc does not grow with decreasing d. For small d, the probability of exceedance $p \to 0.2$ for variant IIc, $p \to$

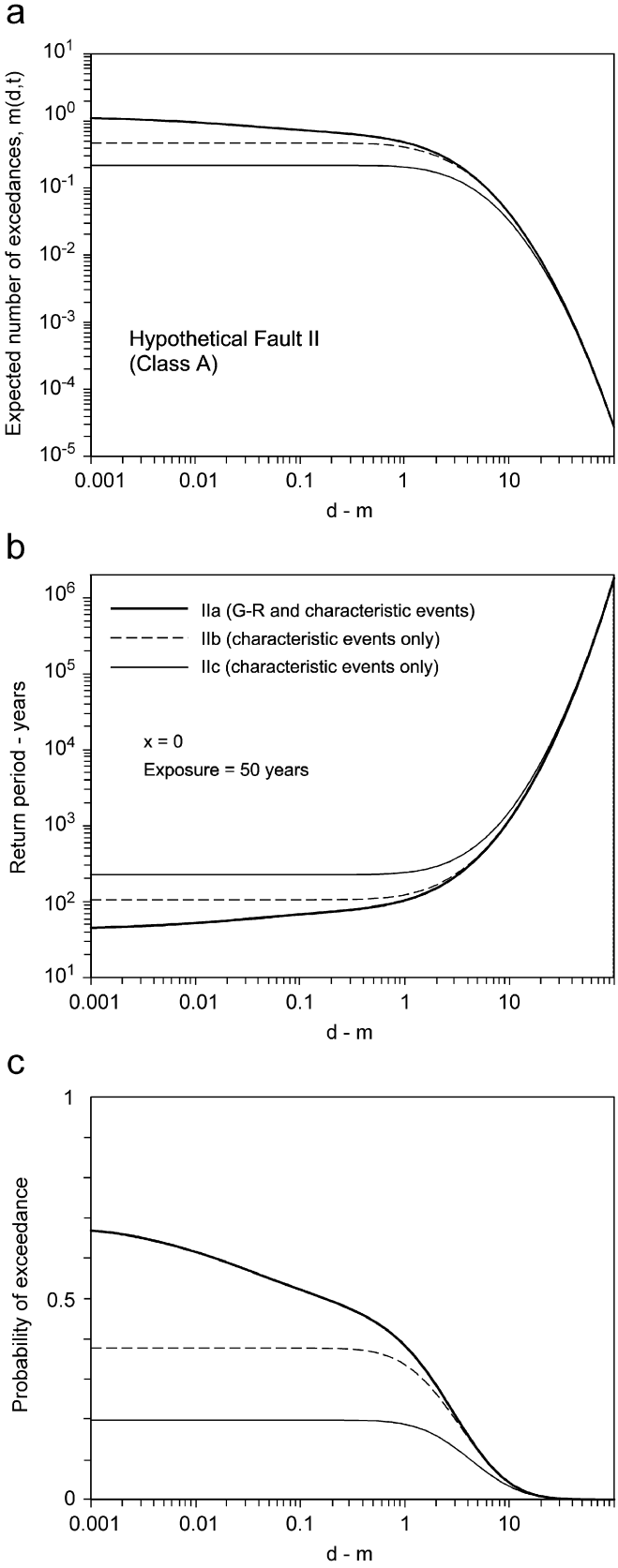

Fig. 8. Results at a site at the center of the fault for hypothetical fault II (Class A): (a) expected number of exceedances of level d during 50 years exposure; (b) return period of exceedance of level d, and (c) probability of exceedance in 50 years. The different lines correspond to different variants of distribution of seismic moment, IIa–IIc.

0.38 for variant IIb, while it continues to grow with decreasing d for variant IIa.

To compare some numbers, for $d = 50\,\text{cm}$, $p = 0.44$ for variant IIa, $p = 0.37$ for variant IIb, and $p = 0.2$ for variant IIa, while $p = 0.1$ for fault I, which has an *order of magnitude* smaller seismic moment rate. For $d = 1\,\text{m}$, $p = 0.38$ for variant IIa, $p = 0.34$ for variant IIb, and $p = 0.19$ for variant IIa, while $p = 0.08$ for fault I. For a large displacement, e.g. $d = 10\,\text{m}$, $p \approx 0.04$ for all variants for fault II, and is insignificant for fault I. In conclusion, Fig. 8 shows that the hazard estimate is quite sensitive to the modeling assumptions affecting the distribution and the number of events over earthquake magnitudes.

10. Discussion and conclusions

A model for the probabilistic assessment of permanent displacement across a fault was presented for applications in design of structures of the transportation systems, such as bridges and tunnels crossing faults. This model is also applicable to other structures crossing faults, such as various pipelines, aqueducts etc. In densely populated regions, such as California, the need for transportation structure to cross an active fault is not uncommon, and often cannot be avoided. Fortunately, certain levels of differential displacement between the supports can be accommodated—by appropriate measures in design. The hazard of permanent differential displacement of the supports of such structures due to a dislocation on the fault is just one adverse consequence of an earthquake, among others that include strong shaking, dynamic differential motion (due to wave passage [22]), large displacements caused by soil liquefaction and settlement, aseismic deformation on the fault caused by creep, etc. The probabilistic approach to the assessment of different hazards provides a mechanism to compare rationally these different hazards, and to compare them with hazards caused by other natural and man made events (e.g. wind, terrorist attacks, etc.). As there is considerable uncertainty in the earthquake occurrence and their effects (more than a factor of 2 in the empirical scaling laws for characteristics of ground shaking), which is not very likely to be significantly reduced during our lifetime, for rational comparison of different consequences from earthquakes, it is essential that the models for the estimation of hazard for different consequences are consistent. This is possible to achieve by using the same seismicity model, and *consistent scaling laws*. This consistency with scaling laws for assessment of various parameters of ground shaking was one of the main objectives in the development of the model presented in this paper.

While conceptually and formally our method is applicable to any region in the world, the particular scaling law used for the displacement across the fault in terms of earthquake magnitude is applicable to faults in California only. The scaling laws we used are consistent with scaling laws for peaks and spectra of strong ground shaking developed by Lee et al. [15], and Lee and Trifunac [16,17] for the California Department of Transportation, City and County of Los Angeles, and with essentially all amplitude scaling relations for strong ground motion [12].

A major difference in the model for assessment of displacement across a fault compared to ground shaking is that, for the latter, many faults even at considerable distance from the site can cause some level of ground shaking, while for the former, not even all events on the fault that is crossed would necessarily affect the site. (In this paper, we are neglecting the co-seismic displacements on a fault caused by nearby earthquakes.) All of these factors lead to smaller probability of exceedance even for very small levels of displacement. For example, for the illustrations in this paper, and for 50 years of exposure, the probability of the displacement exceeding 1 cm is about 0.18 for the hypothetical Class B fault, and is about 0.6, 0.38 and 0.2 for the different choices of distribution of seismic moment for the hypothetical Class A fault.

The illustrations in this paper also show that the results are quite sensitive to how the seismic moment is distributed over earthquake magnitudes, which is mostly based on the judgment of the hazard modeler, or is a result of consensus building (implemented by logic trees [21]), due to insufficient data to determine this more uniquely, and changes with time as more information on the faults becomes available. The trend seen in the illustrations in this paper is that distribution of seismic moment over larger magnitudes may lead to significantly smaller estimates of the hazard (e.g., a factor of two or more for the probability of exceedance of one or several meters of displacement across fault II).

The illustrations in this paper show that the hazard is the largest near the center of the fault and decreases towards the edges. This effect resulted from a hypothetical but physically plausible estimate of the probability that a rupture would extend horizontally to the site, $r_L(M)$, based on the assumption of uniform probability of the rupture occurring anywhere along the fault length as long as it fits within the fault length. The consequences of nonuniform rupture probability along the fault length can be evaluated based on prescribed hypotheses, a priori (e.g. consideration of seismic gaps), by modifying r_W and r_L in Eqs. (13) and (14). We will describe how this is done in future papers. Hence, for the examples illustrated in this paper, the dependence of the hazard on the location of the site along the fault is purely geometric, and depends on the rupture length, which is a function of earthquake magnitude, and on the length of the fault.

The model in this paper assumes that, for a rupture that breaks the surface, the dislocation at the surface is uniform along the entire rupture length. In reality, the dislocation at the surface is nonuniform and may be discontinuous, but the general tendency is that it decreases towards the edges of the rupture [7,14]. Further, a comparison of the adopted model for $D = 2d_{\max}$ with independent data from Wells and Coppersmith [14] for AD and MD surface

displacement (for California faults) shows that our model is more consistent with the data for MD (see Fig. 3).

The model in this paper considers only hazard from earthquakes occurring on the main fault (i.e. the main plane of crustal weakness), which are the main cause for dislocation across the fault. This is referred to as "principal faulting" in Youngs et al. [7], in contrast to "distributed faulting" which can be defined as "the displacement that occurs on other faults, shears, or fractures in the vicinity of the principal rupture in response to the principal faulting…[which is expected to be] discontinuous in nature and may extent outwards several tens of meters to many kilometers from the principal rupture."

For application to a specific fault, it is recommended that, to the extent possible, fault specific (or region specific) information be used to define the probabilities that a rupture will break the ground surface (e.g. based on the distribution of hypocenters) and would extend horizontally to the site, and that most current information is used on the activity of the fault. An interesting problem to be addressed by future research is to compare the hazard for permanent displacement across a fault due to dislocation on the fault with the hazard for dynamic differential motion, and where applicable—with the hazard for differential motion due to consequences of soil liquefaction and lateral spreading.

Acknowledgments

This work was supported by a grant from METRANS, a U.S. Department of Transportation (DOT) designated University Transportation Center (Grant No. 03-27). Its contents reflect the views of the authors, who are responsible for the facts and the accuracy of the information presented herein, and do not necessarily reflect the official views or policies of the U.S. Government or California Department of Transportation. The authors are grateful to Anoosh Shamsabadi from California Department of Transportation, Office of Earthquake Engineering, for the many useful discussions on the application aspect of this project.

References

[1] Shamsabadi A. Personal communication; 2002.
[2] Cao T, Bryant WA, Rowshandel B, Branum D, Wills CJ. The revised 2002 California probabilistic seismic hazard maps; 2003 ⟨http://www.consrv.ca.gov/CGS/rghm/psha/⟩.
[3] Lee VW, Trifunac MD. Microzonation of a metropolitan area, Department of Civil Engineering, Report No. CE 82-02, University of Southern California, Los Angeles, California; 1987.
[4] Trifunac MD. A Microzonation method based on uniform risk spectra. Soil Dyn Earthquake Eng. 1991;9(1):34–43.
[5] Todorovska MI, Trifunac MD. Hazard mapping of normalized peak strain in soil during earthquakes: microzonation of a metropolitan area. Soil Dyn Earthquake Eng. 1996;15(5):321–9.
[6] Todorovska MI, Trifunac MD. Liquefaction opportunity mapping via seismic wave energy. J. Geotech. Geoenviron. Eng. ASC 1999; 125(12):1032–42.
[7] Youngs RR, Arabasz WJ, Anderson RE, Ramelli AR, Ake JP, Slemmons DB, et al. A methodology for probabilistic fault displacement hazard analysis (PFDHA). Earthquake Spectra 2003;19(1):191–219.
[8] Stepp JC, Wong I, Whitney J, Quittmeyer R, Abrahamson N, Torro G. PSHA Project Members. Probabilistic hazard analyses for ground motions and fault displacement at Yucca Mountain, Nevada. Earthquake Spectra 2001;17(1):113–51.
[9] Nishenko SP, Bulland RA. A generic recurrence interval distribution for earthquake forecasting. Bull. Seism. Soc. Am. 1987;77(4): 1382–99.
[10] Todorovska MI. Comparison of response spectrum amplitudes from earthquakes with lognormally and exponentially distributed return period. Soil Dyn Earthquake Eng. 1994;13(2):97–116.
[11] Todorovska MI. Order statistics of functionals of strong ground motion for a class of renewal processes. Soil Dyn Earthquake Eng. 1994;13(6):399–405.
[12] Trifunac MD. Broad band extension of Fourier amplitude spectra of strong motion acceleration. Department of Civil Engineering, Report No. CE 93-01, University of Southern California, Los Angeles, California, 1993.
[13] Trifunac MD. Long period Fourier amplitude spectra of strong motion acceleration. Soil Dyn Earthquake Eng. 1993;12(6):363–82.
[14] Wells DL, Coppersmith KJ. New empirical relationships among magnitude, rupture length, rupture width, rupture area, and surface displacement. Bull. Seism. Soc. Am. 1994;84(4):974–1002.
[15] Lee VW, Trifunac MD, Todorovska MI, Novikova EI. Empirical equations describing attenuation of the peaks of strong ground motion, in terms of magnitude, distance, path effects and site conditions. Report No. 95-02, Department of Civil Engineering, University of Southern California, Los Angeles, California, 1995.
[16] Lee VW, Trifunac MD. Frequency dependent attenuation function and Fourier amplitude spectra of strong earthquake ground motion in California. Report No. CE 95-03, Department of Civil Engineering, University of Southern California, Los Angeles, California, 1995.
[17] Lee VW, Trifunac MD. Pseudo relative velocity spectra of strong earthquake ground motion in California. Department of Civil Engineering, Report No. CE 95-04, University of Southern California, Los Angeles, California, 1995.
[18] Gusev AA. Descriptive statistical model of earthquake source radiation and its application to an estimation of short-period strong motion. Geophys. J. Royal Astr. Soc 1983;74(3):787–808.
[19] Trifunac MD, Novikova EI. Duration of earthquake fault motion in California. Earthquake Eng. Struct. Vib. 1995;2(6):781–99.
[20] Frankel AD, Petersen MD, Mueller CS, Haller KM, Wheeler RL, Leyendecker EV, et al. Documentation for the 2002 update of the national seismic hazard maps. Open File Report 03-420, U.S. Geological Survey, U.S. Department of the Interior, Denver, Colorado, 2002.
[21] Working Group on California Earthquake Probabilities. Earthquake probabilities in the San Francisco Bay region: 2002–2031. Open File Report 03-214, U.S. Geological Survey, U.S. Department of the Interior, Denver, Colorado, 2003.
[22] Trifunac MD, Todorovska MI. Response spectra and differential motion of columns. Earthquake Eng. Struct. Dyn. 1997;26(2):251–68.